Space-time data-driven modeling of precipitation-induced shallow landslides in South Tyrol, Italy

Mateo Moreno[1,2*], Luigi Lombardo[2], Alice Crespi[1], Peter James Zellner[3], Volkmar Mair[4], Massimiliano Pittore[1], Cees van Westen[2], Stefan Steger[1]

Abstract

Shallow landslides represent potentially damaging processes in mountain areas worldwide. These geomorphic processes are usually caused by a combination of predisposing, preparatory, and triggering environmental factors. At regional scales, data-driven methods have been used to model shallow landslides by addressing the spatial and temporal components separately. So far, few studies have explored the integration of space and time for landslide prediction. This research leverages generalized additive mixed models to develop an integrated approach to model shallow landslides in space and time. We built upon data on precipitation-induced landslide records from 2000 to 2020 in South Tyrol, Italy (7,400 km^2). The Slope Unit-based model predicts landslide occurrence as a function of static and dynamic factors while seasonal effects are incorporated. The model also accounts for spatial and temporal biases inherent in the underlying landslide data. We validated the resulting predictions through a suite of cross-validation techniques and tested potential applications. The analysis revealed that the best-performing model combines static ground conditions and two precipitation time windows: short-term cumulative precipitation prior to the landslide event and medium-term cumulative precipitation. We tested the model's predictive capabilities by predicting the dynamic landslide probabilities over hypothetical non-spatially explicit precipitation scenarios and historical precipitation associated with a heavy precipitation event on August 5th, 2016. The novel approach shows the potential to integrate static and dynamic landslide factors for large areas, accounting for the underlying data structure and data limitations.

Keywords: Space-time modeling; GAMMs, Dynamic landslide modeling; Rainfall-induced landslides

[1]Center for Climate Change and Transformation, Eurac Research, Bolzano, Italy

[2]Faculty of Geo-Information Science and Earth Observation (ITC), University of Twente, Enschede, Netherlands

[3]Institute for Earth Observation, Eurac Research, Bolzano, Italy

[4]Office for Geology and Building Materials Testing, Cardano, 39100, Italy

1 Introduction

Landslides are potentially damage-causing geomorphic processes in hilly and mountain areas, which yearly cause thousands of people to lose their lives and belongings (Petley, 2010; Froude and Petley, 2018).

The term "shallow landslide" is generally used to refer to landslides (Cruden and Varnes, 1996; Varnes, 1978; Hungr et al., 2014) in which the sliding surface is located within a depth from a few decimeters up to generally less than two meters (Raetzo et al., 2002). Despite their limited size, shallow landslides can be particularly destructive due to their swift propagation and rapid formation, seemingly lacking pre-event geomorphic evidence (Persichillo et al., 2017).

The occurrence of shallow landslides is driven by a combination of static and dynamic environmental controls. The predisposing factors indicate a location potentially prone to landsliding (e.g., topography, underlying lithology), whereas the preparatory factors (e.g., land cover changes) and triggering factors (e.g., intense precipitation, seismic load) may cause the actual slope failure (Glade et al., 2012; Crozier, 1986). Hence, achieving reliable predictions of landslide occurrence should require a comprehensive consideration of both static and dynamic controls (Corominas et al., 2014).

The selection of an appropriate modeling approach is conditioned by several factors, including the scale of analysis, data quality, and data availability (van Westen et al., 2008; Guzzetti et al., 1999). Specifically, for large areas, data-driven models have been extensively utilized to model shallow landslide occurrences (Reichenbach et al., 2018). However, such assessments have traditionally addressed the spatial component (i.e., *where landslides are likely to occur*) and the temporal component (i.e., *when or under which dynamic conditions landslides are likely to occur*) separately.

In a purely spatial context, data-driven models derive statistical relationships between information on past landslide occurrence (i.e., landslide inventory) and static environmental controls (i.e., predisposing factors) to estimate the spatial likelihood or landslide susceptibility (Brabb, 1984; Guzzetti et al., 2005). The quality of such assessments is strongly influenced by the completeness and quality of the underlying input data. Regional landslide inventories rarely provide a spatially representative sample of past slope instabilities due to the lack of consistent mapping practices throughout an area. This often leads to underrepresented landslide populations (e.g., in areas distant from infrastructure), and consequently, this limitation may introduce bias into the resulting models (Steger et al., 2017; Lima et al., 2021). Such biased models possess restricted practical applicability because they may reflect the methods and underlying assumptions employed during the collection of the landslide inventory. As an illustration, the landslide susceptibility would exhibit probability patterns that correlate with the underlying landslide mapping strategy and the effectively surveyed areas (Bornaetxea et al., 2018; Knevels et al., 2020, i.e., areas explicitly surveyed during the generation of the landslide inventory). To address these challenges, Steger et al. (2021a) proposed novel strategies using generalized additive mixed models (GAMMs) to account for the data collection effects within landslide models.

The assessment of landslide occurrence timing is frequently hindered by the absence of either multi-temporal landslide data or historical records pertaining to triggering events such as rainfall or earthquakes (van Westen et al., 2006; Guzzetti et al., 2012). For large areas, empirical approaches have traditionally been the primary choice for determining critical rainfall conditions for precipitation-induced landslide occurrence (Guzzetti et al., 2007; Glade et al., 2000). These approaches rely on rainfall thresholds derived from past landslide observations (Guzzetti et al., 2007; Kirschbaum and Stanley, 2018) and often serve as the foundation for landslide early warning systems (Segoni et al., 2018a; Gariano et al., 2015). This is achieved by using several representative parameters such as rainfall intensity-duration (Guzzetti et al., 2007), cumulative rainfall event-duration (Peruccacci et al., 2017), and antecedent rainfall conditions (Monsieurs et al., 2019). Conventionally, these approaches adopt a presence-only framework, focusing solely on the rainfall that leads to landslides while disregarding rainfall events that do not trigger landslides. So far, few studies have adopted presence-absence frameworks, which are commonly observed in landslide susceptibility studies, with the distinction that susceptibility solely accounts for static ground-related conditions (e.g., slope steepness, lithology, land cover), while rainfall thresholds are dedicated to the meteorological aspects (Steger et al., 2023; Segoni et al., 2018a). This situation depicts the current separation in the geoscientific literature between two components of the landslide hazard definition (i.e., the "where" and "when" landslides may occur) (Corominas et al., 2014).

The integration of both space and time in data-driven modeling techniques is rarely done (Lombardo and Tanyas, 2020; Samia et al., 2020; Lombardo and Tanyas, 2021; Bajni et al., 2023). Nonetheless, there have been notable endeavors to incorporate dynamic controls into the modeling process by aggregating meteorological factors over specific time periods (e.g., mean annual rainfall; maximum daily rainfall per inventoried period Wang et al., 2022; Dahal et al., 2022). These approaches are better equipped to capture climate variability or long-term meteorological predisposition rather than short-term dynamics. However, by focusing on such long time windows, the impact of extreme events may be diluted or even lost (Camera et al., 2021). The incorporation of intense rainfall into data-driven modeling mainly revolves around event-based assessments and early warning systems (Knevels et al., 2020; Segoni et al., 2018b; Kirschbaum and Stanley, 2018). For instance, Knevels et al. (2020) integrates rainfall by using the maximum rainfall intensity observed within an hourly time window as a predictor within a susceptibility model. In contrast, Segoni et al. (2018b) couples the output of a purely spatial susceptibility model with the results of rainfall threshold exceedance analyses in a heuristic approach to predict landslide occurrence.

To summarize, the integrated modeling of landslides in space and time remains a challenge and is seldom explored in the majority of the geoscientific literature. Its development and application would enhance the understanding of the critical conditions (e.g., rainfall) that lead to slope failure and the quality and reliability of landslide predictions. This research aims to integrate shallow landslide modeling in space and time using data-driven techniques.

Specifically, a binary GAMM is used to account for precipitation as a dynamic predictor at different temporal scales while integrating static landscape characteristics and seasonal effects. We conducted the analysis for a space-time domain covering the territory of South Tyrol (Italy) for 21 years (2000 - 2020).

2 Materials and methods

2.1 Study area

The province of South Tyrol spans approximately 7,400 km^2 and is located in the Eastern Alps, constituting the northernmost part of Italy, as shown in Figure 1. It shares borders with Austria to the north and northeast, Switzerland to the northwest, and the rest of Italy to the south. According to Provincial Statistics Institute (https://astat.provinz.bz.it/) South Tyrol is home to approximately 535,000 people with Bozen, Meran, and Brixen being the most populated municipalities.

The study area is characterized by its diversified geomorphology, geology, and climatic conditions. The landscape is dominated by pronounced variations in altitude (i.e., elevation ranging between ∼200 m and ∼3,900 m a.s.l.) with narrow valleys encompassed by steep slopes. The three main rivers comprise the Rienz River, the Eisack River, and the Etsch River, the latter being Italy's second longest river, flowing eastward into the Adriatic Sea.

Geologically, the area is characterized by the presence of the Periadriatic Line, a major tectonic structure that subdivides the region into two distinct sections: the Southalpine and the Austroalpine (Piacentini et al., 2012). The latter constitutes the western and northern parts of South Tyrol and is mainly composed of metamorphic rocks such as mica schists, amphibolites, orthogneisses, and paragneisses. On the other hand, the Southalpine section, located in the southern and southeastern parts of the study area, is dominated by volcanic rocks, including porphyries, which are covered by carbonatic successions of dolomites and limestones (Stingl and Mair, 2005). Furthermore, the northeastern areas correspond to the Tauren Window, mainly formed by medium-grade calcium-rich metasediments, serpentinites, and metagranitoids as described by Oxburgh (1968).

The climatic conditions exhibit considerable seasonal and spatial variations, predominantly characterized by a continental climate. Airflows of western Atlantic and Mediterranean currents influence the monthly precipitation patterns, as indicated in Crespi et al. (2021); Marra et al. (2014); Adler et al. (2015). The western inner valleys, particularly the Vinschgau Valley, represent the driest areas with an average annual precipitation of ∼500 mm. Conversely, the mountainous areas in the north and northeast experience the highest levels of precipitation, reaching ∼1,500 mm annually. Seasonally, the maximum precipitation is observed during the summer months, with an average of ∼120 mm per month, followed by autumn with ∼80 mm per month. In contrast, winter tends to be the driest period, with an average monthly precipitation of ∼30 mm.

The terrain and climatic settings render this landscape highly prone to landsliding, with predominant failure types belonging to falls, topples, and slides (Schlögel et al., 2020). In South Tyrol, researchers have explored several aspects related to shallow landslides, such as the effects of land use on landslides (Tasser et al., 2003), modeling shallow landslide susceptibility (Piacentini et al., 2012), inventory-based exploratory analysis of landslides (Steger et al., 2021b), the development of strategies to address bias in shallow landslide susceptibility modeling (Steger et al., 2021a), and recent investigations into understanding seasonally dynamic precipitation conditions responsible for shallow landslide occurrence (Steger et al., 2023). However, no regional-scale approach has yet been developed to integrate static and dynamic factors for explaining shallow landslide occurrence in South Tyrol.

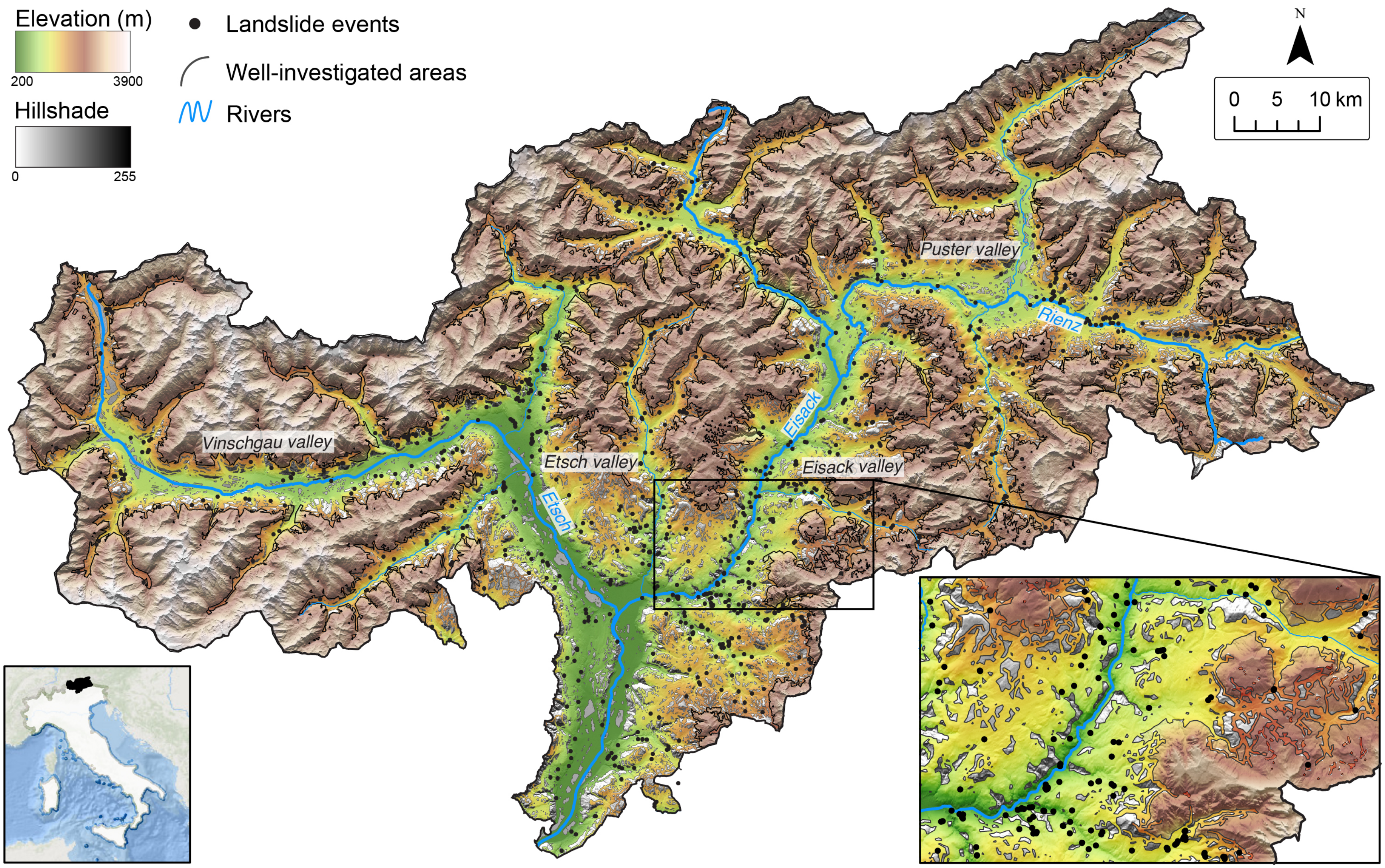

Figure 1: Study area showing the elevation and the filtered landslide scarp locations (n=1006). The dotted line covering the more contrasted zones represents the well-investigated or effectively surveyed areas (i.e., areas with certainty that a landslide is mapped).

2.2 Data

2.2.1 Landslide inventory

The landslide information is extracted from the Italian landslide inventory (*Inventario dei Fenomeni Franosi in Italia*; IFFI), which can be consulted in the IdroGeo platform (https://idrogeo.isprambiente.it/app/). The IFFI project has been coordinated by the Institute for Environmental Protection and Research (ISPRA) since the early years 2000 (Trigila et al., 2007). Each region and autonomous province in Italy is responsible for collecting landslide data for their respective areas of jurisdiction.

In the Autonomous Province of Bolzano, the available point-based information depicts landslide scarp locations which are frequently mapped in the field using Global Positioning Systems (GPS) (Trigila et al., 2010). Landslides that triggered an intervention by the provincial authorities are systematically inventoried, whilst landslides that did not cause any damage (e.g., landslides that occur far from infrastructure) are usually not documented (Steger et al., 2021a). This can be seen in Figure 1, where the well-investigated areas or areas in which landslides are rigorously mapped are highlighted. The inventory shows that up to February 2022, there were 11,416 landslide events and the majority fall into the categories of falls/topples, slides, and flows. Each of these landslides is documented with various attributes that provide detailed information on the movement type, the material involved, the cause, and the occurrence date.

As the primary objective of this study is to dynamically model the probability of landslide occurrences over space and time, specific analyses were supported by selectively extracting from the inventory only those landslide events that were accompanied by the occurrence date information. Further elaboration on this methodical detail is provided in 2.3.

2.2.2 Mapping unit

The selection of the mapping unit is a crucial requirement for any landslide predictive model. Among the most commonly used mapping units, there are pixels (Lima et al., 2021), Slope Units (SUs) (Amato et al., 2019), and unique condition units (Titti et al., 2021), with SU gaining more attention in recent years (Reichenbach et al., 2018). SUs are polygons bounded by streamlines and ridges, reflecting the hydrological and geomorphological processes shaping the natural landscape (Carrara et al., 1991; Guzzetti, 2006). Alvioli et al. (2016) developed an integrated and parametrized GRASS GIS tool known as *r.slopeunits*. This software enables users to generate SU partitions that maximize the polygonal internal homogeneity and external heterogeneity of the slope aspect. To utilize *r.slopeunits*, one needs to provide the Digital Elevation Model (DEM) and specify several parameters such as the circular variance to account for the slope aspect homogeneity, the minimum SU area among others (i.e., flow accumulation threshold and cleansize; for details, see Alvioli et al., 2016). In this research, we chose an SU partition to subdivide the study area. In the process, we intentionally removed the flood plain of the Etsch-Adige River as it can be regarded as a trivial terrain (i.e., easy-to-classify areas in which no landslide is expected; Steger et al., 2016). In the remainder of the manuscript, we also consider other trivial areas, as described in Section 2.3.2. Below, we report the final parameters resulting from multiple iterations in *r.slopeunits* using a bilinearly resampled 30 m LiDAR-DTM (Geokatalog, 2019).

- Circular variance = 0.3
- Minimum Slope Unit area = 500,000 m^2
- Flow accumulation threshold = 1,000,000
- Cleansize = 50,000 m^2

As a result, we obtained a total of 5,379 SUs, whose size distribution has a mean of ∼1.3 km^2 and a standard deviation of ∼0.9 km^2.

2.2.3 Geo-environmental data

This section provides separate descriptions of the static and dynamic landslide controls used to represent the predisposing, preparatory, and triggering factors as summarized in Table 1.

Static factors

Extensive research is available on understanding the different static factors and their relationship to landslide occurrence, as illustrated by Budimir et al. (2015). In this case, we used the bilinearly resampled 30 m LiDAR-DTM to derive common morphological variables such as slope steepness, slope aspect, concavity, local relief, and topographic position index, among others. Geological information was also considered by using the "Geologische Übersichtskarte Südtirol", where the lithological units were grouped into five main classes: (i) crystalline, (ii) porphyry, (iii) sedimentary, (iv) plutonite, and (v) calcschist. More details on the geological information can be found in Steger et al. (2021b). Land cover data were retrieved from "Realnutzungskarte Südtirol v. 2015" and grouped into six classes: (i) agriculture, (ii) forest, (iii) infrastructure, (iv) pasture, (v) rock, (vi) water, and glacier. Moreover, the polygons of the catchment units (i.e., catchment ID) and the topographically corrected SU area (Steger et al., 2021a; Moreno et al., 2023) were also considered during the analysis. In our modeling framework, we further accounted for the effectively surveyed area in order to reduce bias stemming from a spatially uneven registration of past landslides (Bornaetxea et al., 2018; Steger et al., 2021a). This layer (i.e., mask) provides detailed information about the locations where landslides have been meticulously mapped. By including this information, we aimed to limit the inherent spatial bias that may arise from variations in the data collection strategies across different areas (e.g., in areas close or far from infrastructure; see Figure 1).

Dynamic factors

The dynamic factor that primarily influences the timing of shallow landslide occurrences in Italy is precipitation (Brunetti et al., 2010). To capture this important dynamic variable, we utilized the daily precipitation dataset for the Trentino-South Tyrol region, provided by Crespi et al. (2021), which consists of 250-m gridded daily fields. The dataset is computed by interpolating data obtained from a dense network of over 200 meteorological stations, ∼80 of which in South Tyrol, ensuring comprehensive coverage across the study area. The preprocessing of the station data was built upon multiple methodical steps, which involved quality, consistency, and homogeneity tests, as well as gap-filling approaches to maximize series completeness. To account for the influence of the orography on the spatial distribution of precipitation, the interpolation scheme includes a local weighted linear regression with station weights depending on distance and topographic similarity to the target point. The leave-one-out cross-validation returned a mean absolute error (MAE) of 1.1 mm, as averaged across all the meteorological stations and months. Each precipitation field within the dataset represents the total precipitation accumulated over a 24-hour period, specifically from 08:00 UTC of the day before the observation to 08:00 UTC of the observation day (Crespi et al., 2021). In addition to precipitation, the day of the year (DoY) was included as a dynamic predictor. DoY is a sequential number representing each day during a year, starting from 1 on January 1^{st} and ending with 365-366 on December 31^{st}. This value is derived from the assigned date of each SU, and it mainly serves as a proxy for capturing seasonal effects, e.g., vegetation or temperature changes (Steger et al., 2023).

Table 1: Static and dynamic predictor summary table. Continuous properties were aggregated at the SU level by calculating the average value, while categorical properties were aggregated by determining the proportion of each class and the predominant class.

Predictor	Unit	Value	Reference
Slope steepness	degrees	average	(Zevenbergen and Thorne, 1987)
Relief	m	n.a.	(Mark, 1975)
Concavity	%	average	(Iwahashi and Pike, 2007)
Lithology	1	majority	
Land cover	%	proportion	
Catchment ID	1	majority	
Effectively surveyed area	1	average	(Bornaetxea et al., 2018; Steger et al., 2021a)
Slope Unit area	ha	sum	(Moreno and Steger, 2023)
Day of the year	1	n.a.	(Steger et al., 2023)
Year	1	n.a.	(Steger et al., 2023)
Daily precipitation	mm	average	(Crespi et al., 2021)

2.3 Methods

The methodical framework depicted in Figure 2 is divided into three main stages. The first stage encompasses the analysis of static predisposing factors, which resulted in the estimation of landslide susceptibility. The dynamic component was then analyzed in a second stage, yielding the best two precipitation time windows in terms of preparatory and triggering precipitation. Ultimately, the outcomes of the first two stages are integrated to develop a dynamic landslide model accounting for static conditions, the dynamics of precipitation, and seasonal effects. In the following subsection, the three stages are described, along with background information on the GAMMs we implemented.

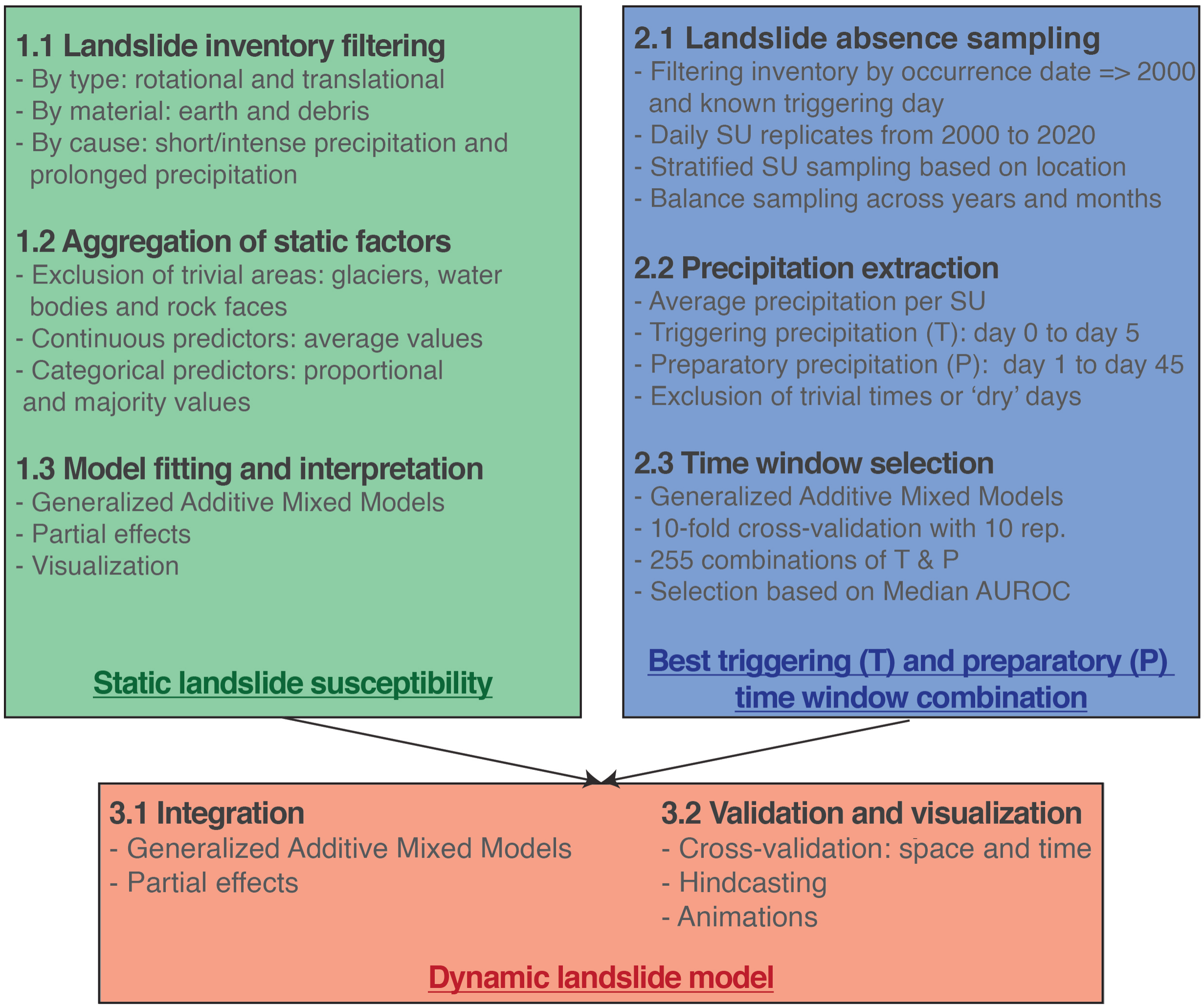

Figure 2: Methodical approach divided into the three main stages we explored in this work: (i) the static component, (ii) the precipitation component, and (iii) the dynamic landslide model.

2.3.1 Modeling landslides using Generalized Additive Mixed Models

GAMMs are a flexible extension of the well-known generalized linear model (GLM) framework. The latter offers the ability to fit a number of exponential probability distributions (e.g., Poisson, Gamma, Gaussian, among others) as a function of a predictor set (Zuur et al., 2009). However, binomial GLMs based on a logit function (i.e., logistic regression) restrict the relation between the response and the independent predictors to the linear case. Although this assumption might be reasonable in some cases, it may not hold for many natural processes. For instance, shallow landslides are known to be nonlinearly dependent on slope steepness because terrains with low and very high slope angles (i.e., with no soil cover) may not host failures, while terrains with middle steepness are naturally prone. In the context of multivariable statistical analyses, GAMMs demonstrate their strength, particularly in these situations, enabling nonlinear effects to be incorporated into the modeling procedure (Wood, 2006; Bolker et al., 2009). In the case of susceptibility studies, this is achieved by assuming that landslide presences and absences are distributed over space and time according to a binomial probability distribution.

We use this modeling framework in the three stages shown in Figure 2. The first one is equivalent to a traditional landslide susceptibility, with only static information appearing in the binomial GAMM to explain the distribution of landslides purely in space as presented in Section 2.3.2. The second stage also corresponds to a binomial GAMM, but this time, only dynamic predictors are featured, aiming at explaining landslide occurrence in time purely from the meteorological perspective and accounting for seasonality (e.g., including a day of the year predictor). This operation is closely linked to Steger et al. (2023) and is intended to estimate the best combination of triggering and preparatory precipitation time windows to explain landslide occurrence. More details on this stage are presented in Section 2.3.3. Ultimately, the outcomes of the two previous stages are integrated into a third stage to produce a unified dynamic landslide prediction model as explained in Section 2.3.4. This model jointly presents temporally invariant ground conditions and precipitation characteristics that are changing dynamically as a function of time.

Notably, binomial models are common in the literature, and assessing their classification performance has been explored in depth. The Receiver Operating Characteristic (ROC) belongs to the class of cutoff-independent metrics and is the most commonly used to distinguish how well a binary classifier performs (Hosmer et al., 2013). We consider the area under the ROC curve (AUROC, hereafter) as a metric to assess the model performance (Faraggi and Reiser, 2002).

2.3.2 Static component

Landslide inventory filtering

We narrowed down the initial landslide data by applying three criteria: (i) movement type, (ii) material type, and (iii) cause type. As a result, we obtained a subset of 1,821 landslides characterized by *translational* and *rotational* movement types, involving *earth* and *debris* materials, and triggered by *short-intense precipitation* or *prolonged precipitation*.

Static factor aggregation

In this study, we utilized the SUs to aggregate both the target variable, which comprises landslide observations, and the predisposing factors previously described in Section 2.2.3. The continuous predictors were aggregated by calculating the average values per SU. Regarding the categorical predictors, we adopted a distinct aggregation method for the geological and land use information. To capture the categorical information of geology within each SU, we implemented the majority rule approach. This method involved identifying the predominant lithotype that covered the majority of the SU polygon. This decision was motivated by the spatial coarseness of geological units, where calculating lithology percentages per SU usually resulted in binary outcomes of either 0% or 100%. Conversely, the land cover layer displayed higher spatial variability, with frequent transitions between different classes. To account for this, we treated the land cover information as a continuous variable, expressed as a percentage of a given class intersecting the SU layer.

Furthermore, the land cover data provided valuable insights for identifying and excluding other trivial terrains, such as rocky faces, glaciers, and water bodies. These areas were excluded from the aggregation process by masking out pixels not classified as trivial terrains. In other words, we performed the aggregation considering only the pixels outside the trivial terrains. By excluding these areas, we aimed to render the classification problem more topic-specific by a priori excluding terrain that does not induce shallow landslides.

Moreover, for the calculation of areal properties (i.e., SU area and proportion of land cover classes), we implemented a correction procedure. This correction aimed to account for potential underestimation caused by the use of conventional planar projection in steep terrains. By applying this correction, we obtained more accurate surface area measurements and mitigated any distortions introduced by the projection method (Steger et al., 2021a; Moreno et al., 2023).

Model fitting and interpretation

We initially fitted a binomial GAMM to the filtered landslide data (i.e., 1,821 landslide observations) using the static predictor set. The layer representing the *effectively surveyed area* was utilized to account for potential biases in the final susceptibility map. A detailed description of the predictor effects can be found in Section 3.1.1. The bias removal procedure we employed can be summarized as follows: Considering that the mapping of landslides in the province is systematic only close to infrastructure, we incorporated a predictor that describes the potential areas that the geological office systematically surveys in South Tyrol on the basis of previously modeled landslide data-collection effects (Steger et al., 2021a). This predictor, referred to as the *effectively surveyed area* (Bornaetxea et al., 2018), was included to capture the spatial variability in the data caused by the spatial mapping bias. By including the *effectively surveyed area*, we ensured that this specific bias was accounted for, enabling the determination of other predictor effects without its confounding influence. To generate an unbiased susceptibility map, we opted to remove the effect of the *effectively surveyed area* from the predictive function. This step constituted one of the two elements involved in the third stage of the analysis detailed in Section 2.3.4).

2.3.3 Precipitation component

Landslide absence sampling

We further filtered the landslide inventory by considering only landslide events with a known date of occurrence, resulting in a final sample size of 676 landslide records. Retrieving this information is a straightforward process. However, sampling the landslide absence information poses a much more complex challenge. Opting for a temporal unit of a single day leads to a substantial increase in the potential number of SUs in both space and time (i.e., approximately forty million = 5,379 SU × 21 years × 365 days). Therefore, a crucial requirement is to extract a suitable number of representative stable SU from this extensive spatiotemporal dataset. To fulfill this requirement, we employed a suitability criterion based on the method proposed in Steger et al. (2023), that encompasses the following elements:

1. Balanced sampling across SUs;
2. Balanced sampling across years;
3. Balanced sampling across months.

We implemented the mentioned criteria as follows. Initially, we randomly selected 10 SU replicates for each location from the possible 21-year dataset. This process resulted in an initial stable dataset consisting of 53,790 SUs. However, we noticed that certain years were represented more frequently than others, leading to an uneven temporal distribution. For this reason, we further constrained the selection process to achieve a balanced yearly absence distribution from the potential 40 million cases. This step ensured that the landslide absence data size remained the same, with 53,790 SUs. Although this operation left a consistent distribution of SUs across the study area and over each year, it did not address the uneven proportion of absences at the monthly level. To address this, we repeated the yearly constraint at a finer monthly resolution. As a result, the final dataset comprised 53,790 SUs representing locations where landslides did not occur across the entire province of South Tyrol, spanning each year and each month from 2000 to 2020. The subsequent step required merging the presence and absence data, an operation that returned a spatiotemporal domain made of 54,460 SU (i.e., 670 presences and 53,790 absences).

Precipitation extraction

We initially assigned the corresponding daily precipitation amounts to each of the 54,460 SUs mentioned above. For detailed methodological information regarding precipitation processing and its assignment to a respective mapping unit, please refer to Steger et al. (2023). The precipitation extraction consisted of 46 days of daily precipitation, starting from the given date assigned to the SUs replicates (i.e., day 0) and moving backward 45 days (i.e., day 45). Then, we calculated the daily cumulative precipitation for each SU replicate up to the 46^{th} day. In addition to this operation, we added a subsequent check to exclude the SUs that did not report precipitation in a period before the observation time. In this step, equivalent to the one applied in Section 2.3.2 where we excluded trivial terrains, we opted for excluding trivial or "dry" periods to ensure problem-specific results. Whenever the total cumulative precipitation was estimated below 1.1 mm (i.e., below the MAE resulting from the precipitation dataset cross-validation) in the first two days (i.e., day 0 and day 1), we removed that SU from the analysis. As a result, the overall space-time domain was reduced to 24,466 SUs, out of which 588 corresponded to unstable slopes (i.e., presences) and 23,878 were stable ones (i.e., absences). In summary, the final sample represents the spatiotemporal distribution of rainy observations with and without landslides.

Time window selection of the cumulative precipitation

In line with the rainfall threshold approach observed in landslide early warning systems (Segoni et al., 2014; Wang et al., 2021; Chleborad, 2003), we determined the most appropriate cumulative precipitation time windows from the possible 46 to describe critical landslide conditions. To address this, we employed a binomial GAMM, in which we aimed to predict landslide presences and absences using two precipitation time windows as predictors. One precipitation time window characterizes the short-term triggering precipitation T (i.e., precipitation shortly before the event), and the other, the medium-term preparatory precipitation P (i.e., precipitation prior to T). The predictor T was built considering the cumulative precipitation windows from day 0 to day 5, whereas P was set by considering the cumulative precipitation time windows prior to T and up to day 45. Additionally, to account for potential seasonal effects and interannual data variability, we included a circular spline effect defined for each DoY and an effect defined for each year ($Year$). Unlike other splines, a year exhibits a cyclic temporal characteristic, necessitating a distinct approach. DoY utilized then a cyclic spline that introduces an additional seasonal constraint. Hence, each day within a year exhibits similar performance across the entire spatiotemporal domain, and the effect of the last day of the year is reciprocally dependent on the first day of the year. The predictor $Year$ guarantees that any potential discrepancies in reporting landslide occurrences over different years do not influence the modeled relationships between our predictors of interest and landslide occurrence. Subsequently, the binomial GAMM was iterated over the 255 possible combinations of the predictors P and T. This procedure is explained in detail in Steger et al. (2023). Differently from this previous study, the current one also incorporated a 10-fold random cross-validation step, conducting the procedure 255,000 times. These iterations corresponded to the 255 pairwise combinations, which we bootstrapped 10 times over 10-randomized repetitions for further robustness. We calculated the AUROC at each step throughout the iterations and stored the results. Ultimately, we identified the best pair of triggering and preparatory precipitation time windows to be the highest median AUROC.

2.3.4 Dynamic landslide prediction model

Integration of static and precipitation components

This final modeling step integrates the two components presented in the previous sections.

The temporally invariant susceptibility of the terrain described in Section 2.3.2 is combined with the temporally-varying component pertaining to the best pair of triggering and preparatory precipitation time windows reported in Section 2.3.3 in a single space-time model. We emphasize that we included a methodical procedure in the static component to address the spatial bias resulting from the landslide mapping strategies. Consequently, the actual susceptibility utilized in the dynamic landslide prediction model is unbiased. This static susceptibility map served as a nonlinear effect in the landslide dynamic model. In other words, the susceptibility map consistently conveys the same signal at each temporal replicate, irrespective of the variations in the spatial distribution of stable and unstable SUs.

The dynamic information provided to the model primarily consisted of three additional predictors representing the triggering and preparatory precipitation effects, as well as seasonal variations captured using the DoY predictor, which were employed in a non-linear manner.

Validation and visualization

The extensive spatiotemporal domain offers numerous possibilities for testing the dynamic model results. We conducted a standard 10-fold random cross-validation (RCV), repeated ten times for a total of 100 iterations. In addition, we included random spatial cross-validation (SCV), utilizing a 10-fold structure repeated ten times (Brenning, 2012). We also featured two temporal validation routines to complement the overall model testing. The first corresponded to a 21-fold temporal validation, where one year is excluded at a time for prediction (i.e., leave-one-year-out), and this process is repeated until every year in the dataset has been predicted. Similarly, we performed the same operation at a monthly level, employing a 12-fold temporal validation. In this case, one month is removed at a time to serve as the prediction target, and the routine is repeated until every month within a year has been predicted.

Ultimately, as a demonstration of its capabilities, we also used our dynamic model for simulation purposes. Ideally, one could employ the model to simulate any day of the year and for any desired duration, provided that the precipitation data is available. However, this operation is computationally intensive in practice. In fact, not only does the precipitation data need to be preprocessed but also aggregated at the SU level before this information is incorporated into the dynamic landslide predictive model. Therefore, to showcase a practical application of our model, we generated two specific scenarios, one for a hypothetical case and one for a specific historical precipitation event. In the first case, the scenario includes temporally varying but spatially homogeneous hypothetical precipitation (i.e., with no variations across the landscape) and the other predictors. In the second case, we conducted a hindcast of the event recorded on August 5^{th}, 2016, by incorporating the spatiotemporal precipitation distribution from July 15^{th} to August 15^{th}, 2016.

3 Results

3.1 Static component

This section shows an overview of the model components and the estimated landslide susceptibility.

3.1.1 Model relationships and landslide susceptibility

Figure 3 offers a comprehensive view of the predictor effects we considered in our model. Below, we provide a concise overview of these predictors by describing their partial effects (i.e., assuming all the other predictor contributions to be fixed).

For instance, the predictor *slope steepness* exhibits a positive nonlinear contribution to the estimated landslide probability. At first, it shows a positive increasing effect that escalates until slope inclinations of $\sim 30°$. However, within steeper SUs surpassing $\sim 30°$, this contribution gradually diminishes, ultimately tapering off to zero for slope angles exceeding $\sim 50°$. The characteristic of *concavity* follows a moderately nonlinear trend, suggesting that SUs displaying a moderate degree of concavity (i.e., $\sim 40\% - 50\%$) hold the highest contribution to the estimated shallow landslide susceptibility. Similarly to the *slope steepness*, the effect of *concavity* also shows a gradual reduction, eventually converging to zero when concavity values approach to $\sim 65\%$.

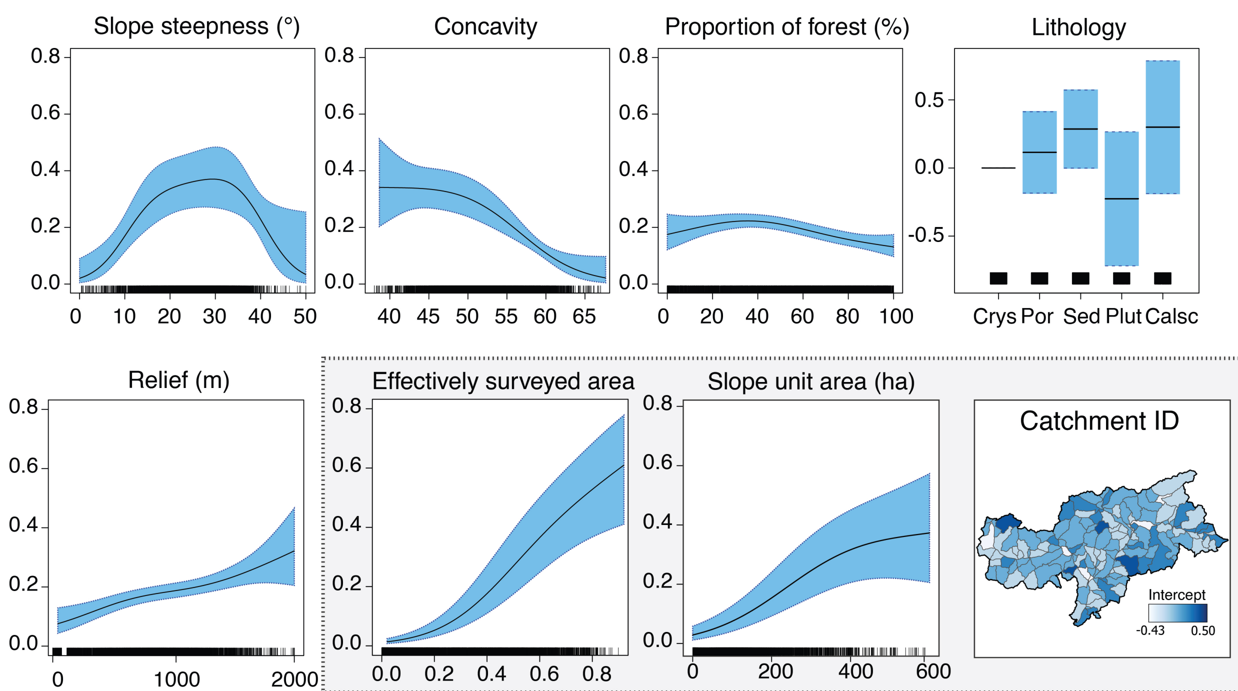

Figure 3: Partial effects of the selected static predictors for the landslide susceptibility estimation. The y-axes are expressed at the response scale probabilities.

Proportion of forest was the only land cover class that showed statistical significance in our model. However, its partial effect seems to remain relatively constant, posing a challenge in describing its specific contribution to landslide susceptibility. Among the scope of the five lithological classes evaluated, a singular distinction emerged in relation to our reference class (i.e., crystalline). Specifically, the "sedimentary rocks" category emerged as statistically significant, positively influencing the estimated landslide susceptibility. The local *relief* exhibited a predominantly linear impact on the model, with its most substantial contributions observed in SUs with relief differences of ∼2000 m.

In addition, three more predictors (i.e., *effectively surveyed area*, *slope unit area*, and *catchment ID*) were included in the model fit but zeroed (i.e., averaged out) from the model predictions. This step ensures that the model isolates their contributions without directly or indirectly reproducing their effects in the predictions. Among these predictors, *effectively surveyed area* had the overall highest contribution to the estimated landslide susceptibility.

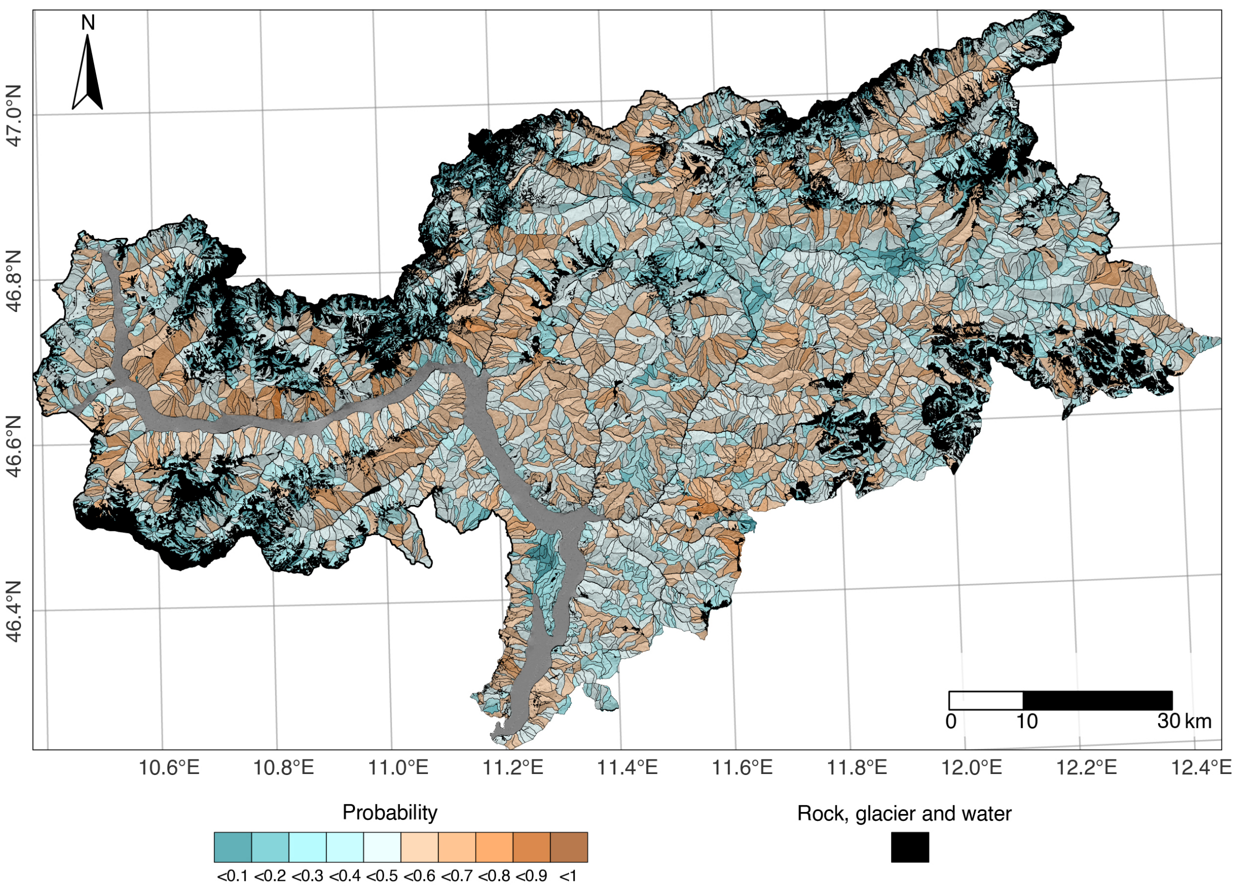

Figure 4: Static landslide susceptibility map. The areas in black consist of the trivial terrains (i.e., rock, glacier, and water bodies). Note that the grey area corresponds to the flood plain of the Etsch-Adige River removed during the SU delineation procedure.

A robust linear trend was evident, illustrating that slopes with high effectively surveyed area scores exerted a considerably greater influence compared to slopes characterized by lower effectively surveyed area scores. For this reason, we removed its effect from the predictions to ensure that our model predictions do not reproduce this effect. Likewise, *slope unit area* displayed a relatively linear trend with positive influences on the estimated susceptibility.

Notably, the SUs characterized by larger areal extents appear to contribute much more to the estimated landslide susceptibility compared to their counterparts with smaller areal extents. By excluding this effect from the predictions, we avoided potentially misleading interpretations that arise from the mapping unit choice.

The map shown in Figure 4 visually presents the spatial distribution of the modeled relationships described in Subsection 3.1.1. This resulting landslide susceptibility model was subsequently integrated with the best precipitation time windows derived in Section 3.2 to construct a dynamic landslide predictive model.

3.2 Precipitation component

The text below presents the results of the best precipitation time windows to describe landslide occurrence.

3.2.1 Time window selection

We utilized the final modeling sample in a 10-fold RCV framework with 10 repetitions to determine the optimal time windows for representing triggering precipitation T and preparatory precipitation P. The pairwise comparison of model performance is depicted in Figure 5a. The combination of T_1 and P_{15} yielded the best performance, with a median AUROC of 0.85. Figure 5b illustrates the practical interpretation of the chosen time windows. T_1 represents a 2-day cumulative precipitation window (i.e., precipitation on day 0 plus day 1), while P_{15} represents a 14-day cumulative precipitation window prior T (i.e., P_{15} minus T_1).

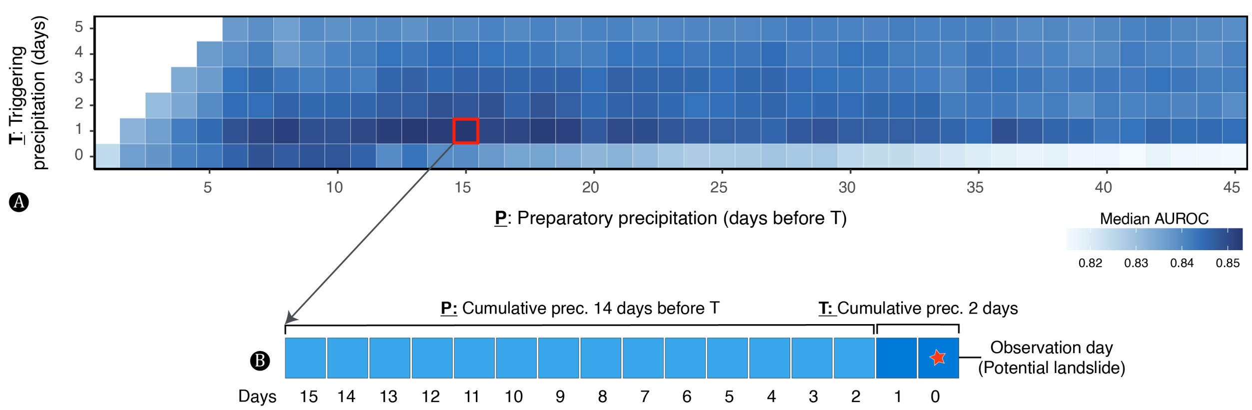

Figure 5: Panel A shows the best combination of precipitation time windows using 10-fold cross-validation with 10 repetitions. The highest AUROC was obtained when combining a triggering precipitation of T_1 and a preparatory precipitation of P_{15}. Panel B shows an interpretation of the best precipitation time windows.

Generally, high AUROCs were achieved when combining the 2-day triggering cumulative precipitation T_1 with preparatory cumulative precipitation ranging from 5 to 20 days (i.e., P_6 to P_{21}). Conversely, lower AUROCs were observed when pairing longer triggering precipitation windows (e.g., T_3 to T_5) with either very long or very short preparatory precipitation windows (e.g., P_0 to P_3 or $> P_{30}$). Additionally, lower performances were observed for almost any combination involving T_0, as this time window only covers 16 hours of the observation day and excludes 8 hours of precipitation considered in subsequent time windows (for more details, see Steger et al., 2023; Crespi et al., 2021).

The resulting best time windows T_1 and P_{15} were then integrated with the static ground conditions modeled in Section 3.1 to construct a dynamic landslide model.

3.3 Dynamic landslide model

In this section, we present an interpretation of the dynamic model components, showcase examples of the estimated probability maps, and discuss the validation of the model.

3.3.1 Model relationships

Figure 6 offers an overview of the components included in the dynamic model. Similarly to the static component, we provide a summary of the predictors by describing their partial effects. The *static susceptibility* exhibits a nonlinear trend, indicating that as the static landslide susceptibility increases, the dynamic landslide probabilities also increase. In terms of the preparatory precipitation P_{15}, its contribution shows a relatively linear behavior. This suggests that as the amount of antecedent 14-day cumulative precipitation increases, the chance of landslide occurrence also increases. Likewise, the triggering precipitation T_1 can be described in a similar manner to the preparatory precipitation. However, it shows notably higher relative probabilities in the domain of high precipitation values. Lastly, it is observed that the predictor DoY indicates slightly lower probabilities around DoY_{200}, corresponding to the summer season.

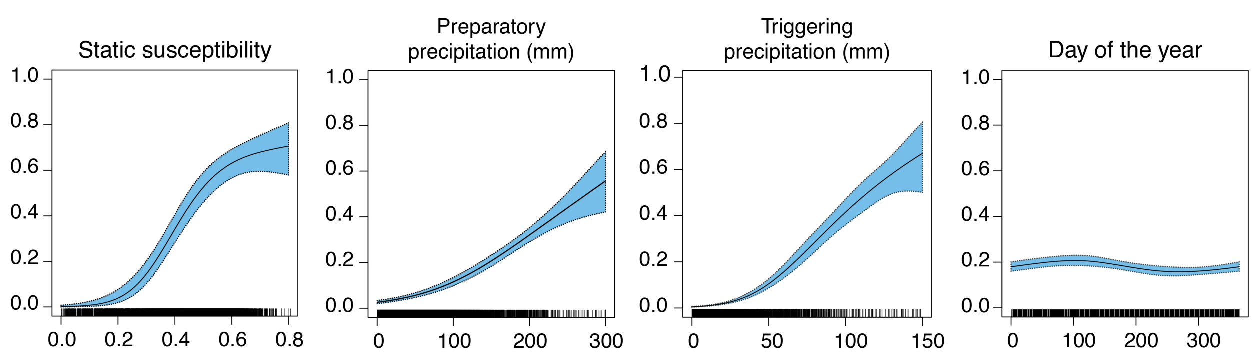

Figure 6: Partial effects of the selected predictors for the dynamic landslide probability estimation. The y-axes are expressed at the response scale probabilities.

3.3.2 Validation and visualization

The validation results are summarized in Figure 7. Overall, the adopted cross-validation approaches depicted a relatively high model generalization and transferability level, with AUROCs consistently above 0.85. This level of performance is considered "excellent discrimination" according to Hosmer et al. (2013).

Regarding the two cross-validation approaches used to assess the spatial component (i.e., RCV and SCV), RCV slightly estimates higher performance scores than SCV. This outcome is expected because SCV eliminates residual dependence from the spatially distributed dataset, providing fair indications where the model does not rely solely on its inherent spatial structure.

In terms of the two cross-validation approaches employed to evaluate the temporal component, we observe nearly identical median AUROCs, but differences arise in terms of uncertainty or the InterQuartile Range (IQR). The larger IQR observed in the "leave-one-year-out" approach can mainly be attributed to the imbalanced distribution of landslide observations across years. Instances with a limited number of landslide observations in specific years may result in poorer predictions for those particular years.

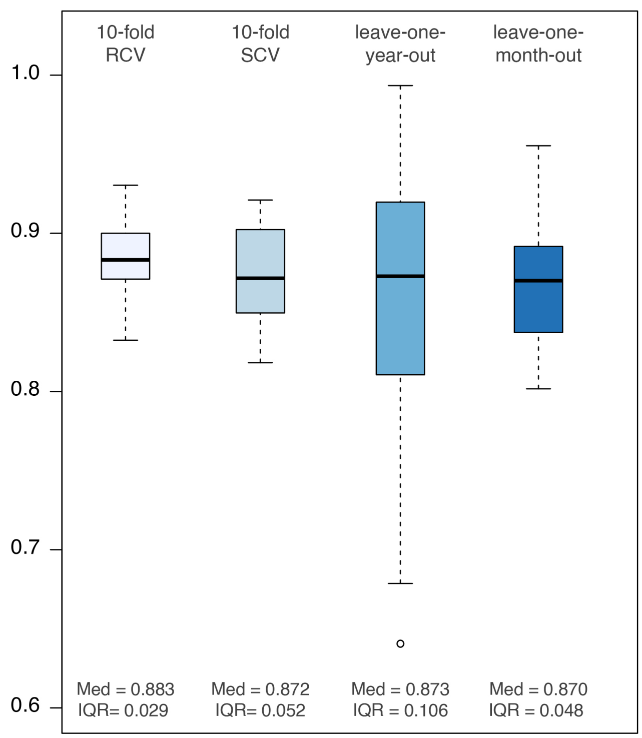

Figure 7: Summary of the model performance featuring the space and time components. The space component is assessed by 10-fold RCV and 10-fold SCV, while the time component is assessed by leave-one-year out and leave-one-month-out validation.

To showcase the model's predictive capabilities, we generated various hypothetical non-spatially explicit triggering T_1 and preparatory P_{15} precipitation scenarios for the study area, as shown in Figure 8. We considered scenarios with 2-day cumulative precipitation values equal to 0, 50, 100, and 150 mm and with P_{15} equal to 15 (i.e., the equivalent to approximately 1 mm of daily precipitation over the past 14 days) and 63 mm. Furthermore, we use the DoY_{200} to 200, corresponding to July 20^{th}, an arbitrary day during the summer season. Through these hypothetical scenarios, the model demonstrates the dynamic changes in shallow landslide probabilities based on (i) the static ground conditions, (ii) both preparatory and triggering precipitation components and (iii) seasonality.

To further demonstrate the versatility of our model, we conducted a hindcast of a heavy localized precipitation event that occurred on the 5^{th} of August 2016. Using the recorded spatiotemporal distribution of precipitation, we generated predictions from the 15^{th} of July to the 15^{th} of August 2016. The resulting predictions are presented as a GIF file, which can be accessed in the supplementary material of this paper. Figure 9 displays two frames from the animation, specifically covering the 4^{th} and 5^{th} of August. These two frames from the animation clearly depict the relatively high probabilities of landslide occurrence predicted by the model in the area where the event occurred, specifically in the Passeier Valley, in the center north of the study area. This highlights the model's capability to hindcast landslides in specific regions, even for localized heavy precipitation events.

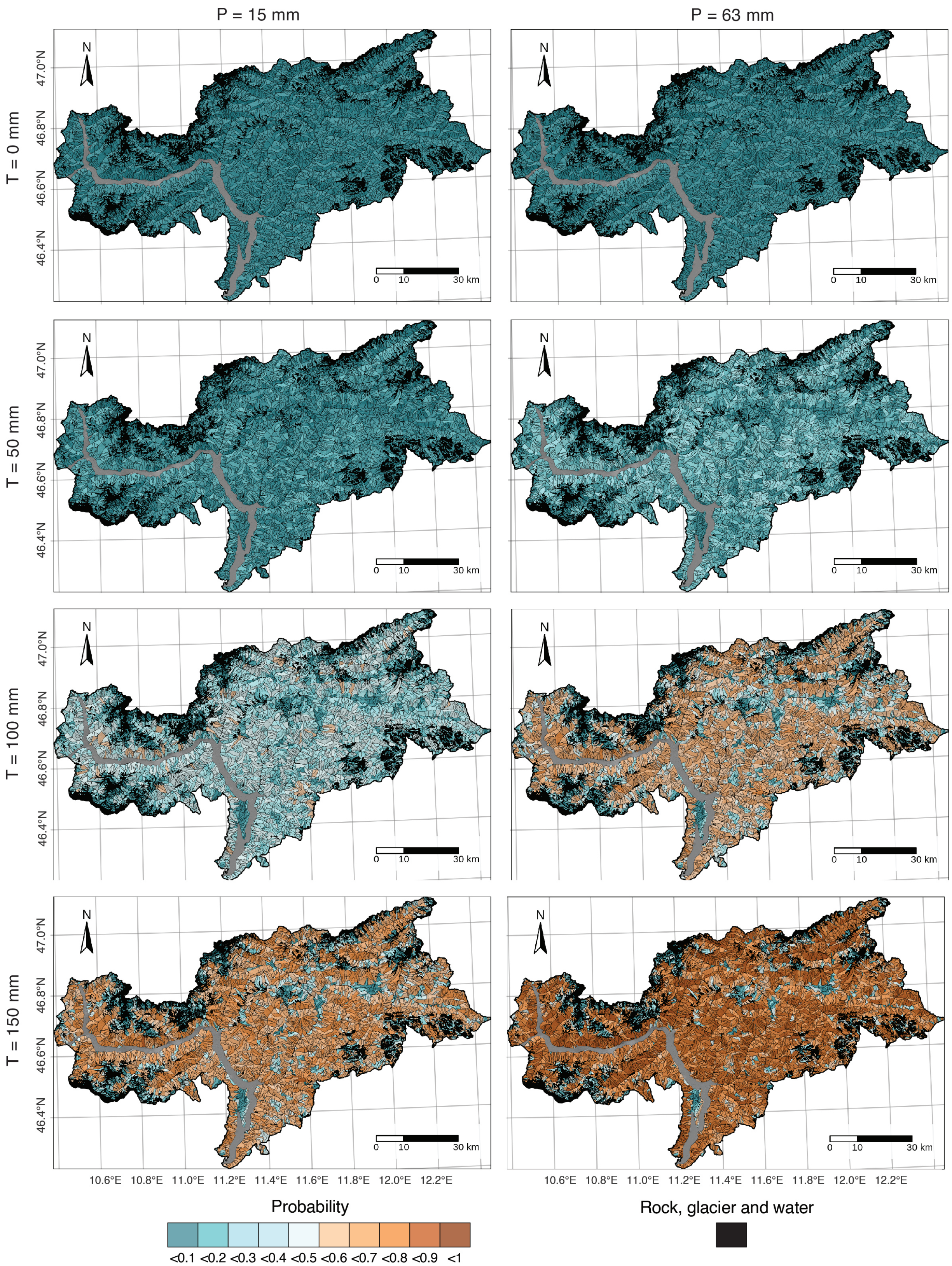

Figure 8: Dynamic landslide predictions with hypothetical non-spatial precipitation scenarios. Preparatory precipitation P_{15} is set to 15 mm and 63 mm, while the triggering precipitation T_1 is set to 0 mm, 50 mm, 100 mm, and 150 mm.

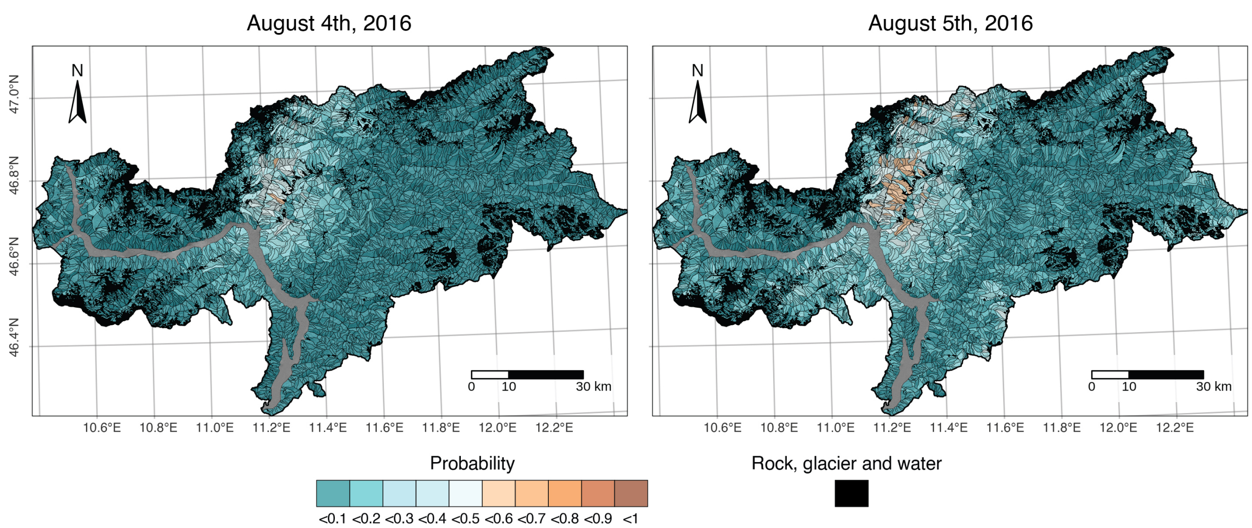

Figure 9: Dynamic landslide predictions for hindcasting landslides associated with precipitation event in the Passeier Valley on the 4^{th} and 5^{th} of August 2016.

4 Discussion

In this research, we developed a data-driven approach to integrate static and dynamic factors for the prediction of precipitation-induced shallow landslides. The resulting model demonstrates a robust performance, consistently achieving AUROCs surpassing 0.85. This reflects the model's capabilities of accounting for static ground conditions, short-term triggering precipitation, medium-term preparatory precipitation, seasonal effects, and spatial biases. The modeled relationships, the model's strengths, limitations, and applications are discussed below.

4.1 Understanding the static and dynamic modeled relationships

Fig. 3, we visualized the partial effects of the statics predictors used when modeling landslide susceptibility. Below, we provide an interpretation of some of the most relevant ones.

The contribution of *slope steepness* to the landslide susceptibility diminishes for inclinations exceeding ∼30°. This reduction can be explained by the prevalence of thin or absent soil layers on exceedingly steep gradients, caused by, e.g., soil erosion caused by rainfall (Chen et al., 2018). Consequently, given that the initial screening of the landslide inventory was centered around landslides with earth or debris materials, the steep slopes characterized by minimal or absent soil will decrease the probability of landslide incidence.

Only the *proportion of forest* depicted statistical significance among the six distinct land cover classes. Nonetheless, the interpretation of its partial effect encounters some considerations. This ambiguity could potentially be ascribed to the presence of confounding factors (e.g., elevation) that influence the relationship between forest cover and landslide occurrence. Additionally, it is plausible that *proportion of forest* exhibits limited variability across the SUs since, in South Tyrol, forested areas tend to dominate the lower elevation slopes while being less prevalent on higher elevation slopes. Given that the mapping units (i.e., SUs) often span a wide elevation range from the toeslope to the summit, they inherently incorporate an average effect of the *proportion of forest*. This consideration may explain the relatively smoothed effect that *proportion of forest* has in the landslide susceptibility.

The strong influence of *effectively surveyed area* suggests the importance of accounting for it in the analyses. This effect signifies that SUs that have been effectively surveyed, particularly those located in proximity to infrastructure, are estimated as more susceptible to landslides when contrasted with their less-investigated counterparts (i.e., SUs with lower effectively surveyed area scores). From a geomorphological standpoint, this trend does not inherently relate to SUs being more or less susceptible. Instead, it reflects the underlying landslide collection strategy referred to as "data collection effects" (Steger et al., 2021a). The landslide inventory for the study area solely encompasses the landslides that prompted interventions by the provincial offices. Consequently, landslides that did not cause any damage or pose any threat (e.g., landslides far from infrastructure) typically go unrecorded. For these reasons, not accounting for this factor and not excluding it within our model would have resulted in an overrepresentation of high susceptible SUs primarily in close proximity to infrastructure while deeming SUs distant from infrastructure as less susceptible.

Similarly, it was found that *slope unit area* substantially influenced the estimated landslide susceptibility. This may lead to the assumption that as the areal extent of the SU becomes larger, the modeled landslide susceptibility also increases. However, this assumption does not hold true because the areal extent of the mapping unit does not necessarily condition whether a terrain is more prone to landsliding. In reality, landslide susceptibility is determined by the interplay of geo-environmental factors and not by the areal extent of the underlying mapping unit. Therefore, neglecting to account for the areal extent of the mapping unit would have resulted in an erroneous estimation, wherein SUs were labeled as more susceptible solely due to their areal extent when compared to their smaller areal extent counterparts. To avoid misleading interpretations caused by the choice of mapping unit, it is important to consider the implications of the areal extent of the SUs.

The majority of the literature dedicated to temporal landslide prediction relies on rainfall thresholds, where the presence-absence framework, which considers only the rainfall events leading to landslides while disregarding those that do not trigger landslides, is frequently overlooked. Our optimal time window selection process results reveal that the combination of time windows yielding the best performance includes T 2-day cumulative precipitation and P 14-day cumulative precipitation preceding T, as illustrated in Fig. 5. Notably, our optimal time window combination, particularly the component pertaining to factor P, exhibited a relatively shorter time window compared to the findings in Steger et al. (2023), where the highest-performing combination involved P with 28-day cumulative precipitation prior to T. We attribute this discrepancy mainly to the choice of mapping unit; we employ SUs, whereas pixels were utilized in the previous study. SUs need an aggregation step due to the gridded structure of precipitation datasets. This aggregation process can result in a more averaged representation of precipitation values compared to pixel-scale analyses. Furthermore, it is worth noting that while the combination with the highest median AUROC involves T_1 and P_{15}, the differences among alternative combinations, such as T_1 and P_{29}, are relatively minor. This suggests that the results are relatively stable and not drastically affected by the choice of a slightly different time window.

Regarding the partial effects observed in the dynamic model, as depicted in Fig. 6, it is noteworthy that while the variable DoY exhibits a relatively consistent pattern, some fluctuations are evident, particularly along DoY_{200}. Importantly, these fluctuations should not be understood as a reduced likelihood of landsliding across the summer months. Rather, they suggest a more nuanced relationship. Specifically, they hint at the intricate interplay between DoY and the characteristic heavy precipitation patterns typical of Alpine summers, which are, to some extent, captured by the predictors T and P. In practical terms, since our model already accounts for the effects of precipitation, it implies that an equal amount of precipitation (e.g., 100 mm of precipitation) results in a lower probability of landslide occurrence during the summer season. This phenomenon may be attributed to the potentially stabilizing influences of vegetation and temperature on slope stability during this particular season, as also discussed in Steger et al. (2023).

4.2 Benefits of a space-time approach

The landslide hazard definition initially proposed by Varnes (1984) and subsequently modified by Guzzetti et al. (1999) requires the evaluation of three critical components: spatial assessment (i.e., determining where landslides may occur), temporal assessment (i.e., identifying when or under which conditions landslides may occur), and intensity assessment (i.e., estimating the potential destructiveness of landslides in a given area). In the context of our approach, although we do not encompass all three components, we do effectively address the spatial and temporal aspects. Notably, in the scientific literature, there is a prevalence of landslide susceptibility studies that predominantly focus on the analysis of static factors, effectively covering the spatial component, as highlighted in Reichenbach et al. (2018) . However, endeavors are scarce to integrate static and dynamic factors or unify the space and time dimensions into a comprehensive model (Lombardo et al., 2020; Wang et al., 2022). Also, as emphasized in the introduction of this manuscript, landslides are the outcome of a complex interplay among predisposing, preparatory, and triggering environmental factors. In this interplay, the stability of a slope is portrayed as a function of these three categories of factors (Crozier, 1986). To illustrate, a slope characterized by predisposing factors contributing significantly to its instability may require only minimal preparatory and triggering factors to become unstable. In the context of our model, a slope characterized by a high landslide susceptibility may demand only limited amounts of medium-term (i.e., P) and short-term (i.e., T) precipitation to undergo failure. Conversely, a slope with low landslide susceptibility may require substantial quantities of medium-term and short-term precipitation to reach a state of instability. In contrast to traditional regional approaches where reclassified landslide susceptibility is combined with reclassified precipitation levels through heuristic methods, our approach harnesses the power of GAMMs to integrate both elements while accounting for nonlinearities.

Another noteworthy aspect to highlight is the high interpretability and high performance that our model affords, largely attributable to the selected GAMM modeling framework. In particular, the partial effect plots offer a great benefit to gaining insights into how static and dynamic environmental factors may, albeit statistically, contribute to the occurrence of landslides in both space and time. The model consistently demonstrates excellent classification results, as evidenced by the robust performance scores across various cross-validation routines, including RCV, SCV, leave-one-year-out, and leave-one-month-out assessments.

The developed approach's practical utility and implementation possibilities are presented in two instances. The first instance, exemplified in Fig. 8, pertained to hypothetical precipitation scenarios. These scenarios allowed for the estimation of landslide dynamic probabilities under varying precipitation conditions, either with or without spatial variation. In our specific illustration, we opted for non-spatially explicit precipitation conditions. In this manner, the outcomes reveal notable differences in the estimated dynamic landslide probabilities between scenarios with relatively low preparatory precipitation and those with high preparatory precipitation, with the latter being much more drastic. In the second instance exemplified in 9, we evaluated our model during a localized, heavy precipitation event that occurred between the 4^{th} and 5^{th} of August 2016. The results consistently demonstrate the model's ability to predict relatively high landslide probabilities within the affected areas during this period.

Furthermore, our approach holds promise for other applications in the realm of early warning systems. By extending the approach developed in Steger et al. (2023) to encompass the space-time framework outlined here, it becomes feasible to utilize dynamic precipitation thresholds while also accounting for static terrain factors. This extension entails assessing whether observed or anticipated precipitation amounts are likely to exceed specific thresholds established for particular terrain and seasonal conditions, such as steep slopes, forested terrain, or low elevations in summer or winter.

4.3 Limitations and future work

As previously mentioned in the discussion of the model's benefits, it is important to emphasize that a comprehensive landslide hazard assessment needs to consider the evaluation of landslide intensity as one key component. Although our developed approach addresses spatial and temporal aspects, it currently lacks the capability to assess intensity. Consequently, it cannot provide an estimation of landslide hazard, which is a crucial part for conducting landslide risk assessment.

Additionally, our approach relies on high-resolution gridded precipitation data sourced from Crespi et al. (2021). However, these data may not be readily available or easily obtainable if one were to extend the approach to different geographic regions. In such cases, the use of satellite-based precipitation products, as implemented in other recent research studies (Kirschbaum et al., 2015; Kirschbaum and Stanley, 2018; Stanley et al., 2021), could offer a viable alternative.

Furthermore, the selection of the mapping unit posed certain challenges, particularly with respect to the aggregation of predictors. This aggregation process proved to be computationally costly and raised issues, particularly when dealing with static predictors. Those inherent issues arise from the fact that a SU encompasses a spatial domain spanning from the toeslope to the summit. Consequently, aggregating these predictors often leads to undesirable over-smoothing effects, as was evident in the case of the *proportion of forest*. In light of these challenges, we advocate for further research within the domain of SU-based landslide models, focusing on the development of appropriate aggregation strategies tailored to specific predictor variables or identifying sets of predictors that do not exhibit these excessive smoothing effects. This research direction will be instrumental in improving the accuracy and interpretability of such models in the future.

Moreover, concerning the aggregation of precipitation data, this workflow proved to be relatively time-consuming. Specifically, the precipitation extraction process for the 53,790 SUs required approximately 16 hours to complete. This demanding task was executed using the ITC Geospatial Data Analysis Platform https://crib.utwente.nl/ with a computing configuration featuring 72 vCPU Intel x86-64/768 GB RAM/NVIDIA RTX A4000 GPU.

Our future research endeavors will center on the integration of additional dynamic predictors, which includes an examination of the intricate relationships between precipitation, temperature, and snow (Camera et al., 2021; Bajni et al., 2023). We plan to expand our investigations by extending our model framework to sub-daily precipitation measurements, which can be derived from meteorological RADAR observations. This finer temporal resolution in precipitation data can provide valuable insights into short-term variations and their influence on landslide occurrences. Another important aspect to explore involves evaluating the predictive capabilities of our model under various projected precipitation scenarios, particularly in the context of climate change. This step may help us understand how our approach performs under altered precipitation patterns, which are anticipated to become increasingly relevant in the future. Furthermore, we aim to enhance our model by integrating an intensity estimation component. In theory, this integration may enable offering a complete assessment of landslide hazard, thereby advancing our ability to assess and reduce landslide risk effectively.

5 Conclusion

We have presented a novel approach employing GAMMs to effectively integrate static ground conditions and dynamic preparatory and triggering factors for the prediction of shallow landslides in both space and time within South Tyrol in the northeastern Italian Alps from 2000 to 2020. The static predisposing factors, featured by the *static susceptibility* predictor, are integrated with dynamic factors such as daily cumulative precipitation represented by medium-term precipitation, short-term precipitation, and the day of the year to account for seasonal variations. Additionally, our SU-based approach addresses critical issues related to spatial biases in landslide inventory, potential reporting biases across different years, and the areal extent of the chosen mapping unit. Through a comprehensive multi-validation strategy in both space and time, our model consistently exhibited excellent predictive performance, consistently achieving AUROC values above 0.85. Moreover, we have demonstrated the practical applicability of our approach in two specific scenarios. Firstly, we employed our approach to estimate landslide probabilities under hypothetical precipitation scenarios. Secondly, we successfully utilized the model for hindcasting, effectively reproducing landslides triggered by heavy and localized precipitation events. These applications underscore the real-world utility of our approach in enhancing landslide prediction and extending it into space and time.

Acknowledgement

We thank the Faculty of Geo-information Science and Earth Observation (ITC), University of Twente, for covering the open-access publication costs. The authors also thank the Provincial Office for Geology and Building Materials Testing of the Autonomous Province of Bozen-Bolzano for their assistance in the preparation of landslide data. The research leading to these results is framed within the PROSLIDE project - integration of static and dynamic landslide controls at multiple scales using data-driven and physically-based methods – exploring new opportunities for the PRediction Of shallow landSLIDEs (https://www.mountainresearch.at/proslide/) that received funding from the research program Research Südtirol-Alto Adige 2019 of the Autonomous Province of Bozen-Bolzano – Südtirol-Alto Adige.

References

Adler, S., Chimani, B., Drechsel, S., Haslinger, K., Hiebl, J., Meyer, V., Resch, G., Rudolph, J., Vergeiner, J., Zingerle, C., Marigo, G., Fischer, A. and Seiser, B. (2015) Das Klima: Von Tirol-Sudtirol-Belluno. Technical report, ZAMG, Autonome Provinz Bozen, ARPAV.

Alvioli, M., Marchesini, I., Reichenbach, P., Rossi, M., Ardizzone, F., Fiorucci, F. and Guzzetti, F. (2016) Automatic delineation of geomorphological slope units with r.slopeunits v1.0 and their optimization for landslide susceptibility modeling. Geoscientific Model Development **9**(11), 3975–3991.

Amato, G., Eisank, C., Castro-Camilo, D. and Lombardo, L. (2019) Accounting for covariate distributions in slope-unit-based landslide susceptibility models. a case study in the alpine environment. Engineering geology **260**, 105237.

Bajni, G., Camera, C. A. and Apuani, T. (2023) A novel dynamic rockfall susceptibility model including precipitation, temperature and snowmelt predictors: a case study in aosta valley (northern italy). Landslides pp. 1–24.

Bolker, B. M., Brooks, M. E., Clark, C. J., Geange, S. W., Poulsen, J. R., Stevens, M. H. H. and White, J. S. S. (2009) Generalized linear mixed models: a practical guide for ecology and evolution. Trends in Ecology & Evolution **24**(3), 127–135.

Bornaetxea, T., Rossi, M., Marchesini, I. and Alvioli, M. (2018) Effective surveyed area and its role in statistical landslide susceptibility assessments. Natural Hazards and Earth System Sciences **18**(9), 2455–2469.

Brabb, E. (1984) Innovative approaches to landslide hazard and risk mapping. In Proceedings of IVth International Conference and Field Workshop in Landslides, volume 1, pp. 307–324. Toronto, Canada: .

Brenning, A. (2012) Spatial cross-validation and bootstrap for the assessment of prediction rules in remote sensing: The r package sperrorest. In 2012 IEEE international geoscience and remote sensing symposium, pp. 5372–5375.

Brunetti, M. T., Peruccacci, S., Rossi, M., Luciani, S., Valigi, D. and Guzzetti, F. (2010) Rainfall thresholds for the possible occurrence of landslides in italy. Natural Hazards and Earth System Sciences **10**(3), 447–458.

Budimir, M., Atkinson, P. and Lewis, H. (2015) A systematic review of landslide probability mapping using logistic regression. Landslides **12**, 419–436.

Camera, C. A., Bajni, G., Corno, I., Raffa, M., Stevenazzi, S. and Apuani, T. (2021) Introducing intense rainfall and snowmelt variables to implement a process-related non-stationary shallow landslide susceptibility analysis. Science of the Total Environment **786**.

Carrara, A., Cardinali, M., Detti, R., Guzzetti, F., Pasqui, V. and Reichenbach, P. (1991) GIS techniques and statistical models in evaluating landslide hazard. Earth Surface Processes and Landforms **16**(5), 427–445.

Chen, H., Zhang, X., Abla, M., Lü, D., Yan, R., Ren, Q., Ren, Z., Yang, Y., Zhao, W., Lin, P. et al. (2018) Effects of vegetation and rainfall types on surface runoff and soil erosion on steep slopes on the loess plateau, china. Catena **170**, 141–149.

Chleborad, A. F. (2003) Preliminary evaluation of a precipitation threshold for anticipating the occurrence of landslides in the seattle, washington. Technical report, U.S. Geological Survey.

Corominas, J., van Westen, C., Frattini, P., Cascini, L., Malet, J. P., Fotopoulou, S., Catani, F., Van Den Eeckhaut, M., Mavrouli, O., Agliardi, F., Pitilakis, K., Winter, M. G., Pastor, M., Ferlisi, S., Tofani, V., Hervás, J. and Smith, J. T. (2014) Recommendations for the quantitative analysis of landslide risk. Bulletin of Engineering Geology and the Environment **73**(2), 209–263.

Crespi, A., Matiu, M., Bertoldi, G., Petitta, M. and Zebisch, M. (2021) A high-resolution gridded dataset of daily temperature and precipitation records (1980-2018) for Trentino-South Tyrol (north-eastern Italian Alps). Earth System Science Data **13**(6), 2801–2818.

Crozier, M. (1986) Landslides: Causes, Consequences & Environment. Croom Helm. ISBN 9780709907909.

Cruden, D. M. and Varnes, D. J. (1996) Landslide types and processes. Number 247 in Special report National Research Council (U.S.). Washington D.C.: Transportation Research Board. ISBN 030906208X.

Dahal, A., Tanyas, H., van Westen, C. J., van der Meijde, M., Mai, P. M., Huser, R. and Lombardo, L. (2022) Space-time landslide hazard modeling via ensemble neural networks .

Faraggi, D. and Reiser, B. (2002) Estimation of the area under the ROC curve. Statistics in medicine **21**(20), 3093–3106.

Froude, M. J. and Petley, D. N. (2018) Global fatal landslide occurrence from 2004 to 2016. Natural Hazards and Earth System Sciences **18**(8), 2161–2181.

Gariano, S. L., Brunetti, M. T., Iovine, G., Melillo, M., Peruccacci, S., Terranova, O., Vennari, C. and Guzzetti, F. (2015) Calibration and validation of rainfall thresholds for shallow landslide forecasting in sicily, southern italy. Geomorphology **228**, 653–665.

Geokatalog (2019) Open Geodatabase of the Autonomous Province of South Tyrol.

Glade, T., Anderson, M. and Crozier, M. J. (2012) Landslide Hazard and Risk. Wiley Blackwell. ISBN 9780470012659.

Glade, T., Crozier, M. and Smith, P. (2000) Applying probability determination to refine landslide-triggering rainfall thresholds using an empirical "antecedent daily rainfall model". Pure and Applied Geophysics **157**, 1059–1079.

Guzzetti, F. (2006) Landslide hazard and risk assessment. Ph.D. thesis, University of Bonn, Bonn, Germany.

Guzzetti, F., Carrara, A., Cardinali, M. and Reichenbach, P. (1999) Landslide hazard evaluation: A review of current techniques and their application in a multi-scale study, Central Italy. Geomorphology **31**(1-4), 181–216.

Guzzetti, F., Mondini, A. C., Cardinali, M., Fiorucci, F., Santangelo, M. and Chang, K. T. (2012) Landslide inventory maps: New tools for an old problem.

Guzzetti, F., Peruccacci, S., Rossi, M. and Stark, C. P. (2007) Rainfall thresholds for the initiation of landslides in central and southern Europe. Meteorology and atmospheric physics **98**, 239–267.

Guzzetti, F., Reichenbach, P., Cardinali, M., Galli, M. and Ardizzone, F. (2005) Probabilistic landslide hazard assessment at the basin scale. Geomorphology **72**(1-4), 272–299.

Hosmer, D. W., Lemeshow, S. and Sturdivant, R. X. (2013) Applied Logistic Regression: Third Edition. Applied Logistic Regression: Third Edition pp. 1–510.

Hungr, O., Leroueil, S. and Picarelli, L. (2014) The Varnes classification of landslide types, an update.

Iwahashi, J. and Pike, R. J. (2007) Automated classifications of topography from dems by an unsupervised nested-means algorithm and a three-part geometric signature. Geomorphology **86**(3-4), 409–440.

Kirschbaum, D. and Stanley, T. (2018) Satellite-based assessment of rainfall-triggered landslide hazard for situational awareness. Earth's Future **6**(3), 505–523.

Kirschbaum, D., Stanley, T. and Zhou, Y. (2015) Spatial and temporal analysis of a global landslide catalog. Geomorphology **249**, 4–15.

Knevels, R., Petschko, H., Proske, H., Leopold, P., Maraun, D. and Brenning, A. (2020) Event-based landslide modeling in the Styrian basin, Austria: Accounting for time-varying rainfall and land cover. Geosciences 2020, Vol. 10, Page 217 **10**(6), 217.

Lima, P., Steger, S. and Glade, T. (2021) Counteracting flawed landslide data in statistically based landslide susceptibility modelling for very large areas: a national-scale assessment for austria. Landslides **18**(11), 3531–3546.

Lombardo, L., Opitz, T., Ardizzone, F., Guzzetti, F. and Huser, R. (2020) Space-time landslide predictive modelling.

Lombardo, L. and Tanyas, H. (2020) Chrono-validation of near-real-time landslide susceptibility models via plug-in statistical simulations. Engineering Geology **278**.

Lombardo, L. and Tanyas, H. (2021) From scenario-based seismic hazard to scenario-based landslide hazard: fast-forwarding to the future via statistical simulations. Stochastic environmental research and risk assessment pp. 1–14.

Mark, D. M. (1975) Geomorphometric Parameters: A Review and Evaluation. Geografiska Annaler. Series A, Physical Geography **57**(3/4), 165.

Marra, F., Nikolopoulos, E. I., Creutin, J. D. and Borga, M. (2014) Radar rainfall estimation for the identification of debris-flow occurrence thresholds. Journal of Hydrology **519**(PB), 1607–1619.

Monsieurs, E., Dewitte, O. and Demoulin, A. (2019) A susceptibility-based rainfall threshold approach for landslide occurrence. Hazards Earth Syst. Sci **19**(4), 775–789.

Moreno, M. and Steger, S. (2023) Slope unit size matters-why should the areal extent of slope units be considered in data-driven landslide susceptibility models? In EGU General Assembly 2023.

Moreno, M., Steger, S., Tanyas, H. and Lombardo, L. (2023) Modeling the area of co-seismic landslides via data-driven models: The kaikōura example. Engineering Geology **320**, 107121.

Oxburgh, E. R. (1968) An outline of the geology of the central eastern alps. Proceedings of the Geologists' Association **79**(1), 1–IN2.

Persichillo, M. G., Bordoni, M. and Meisina, C. (2017) The role of land use changes in the distribution of shallow landslides. Science of The Total Environment **574**, 924–937.

Peruccacci, S., Brunetti, M. T., Gariano, S. L., Melillo, M., Rossi, M. and Guzzetti, F. (2017) Rainfall thresholds for possible landslide occurrence in italy. Geomorphology **290**, 39–57.

Petley, D. (2010) Landslide hazards. Geomorphological Hazards and Disaster Prevention pp. 63–74.

Piacentini, D., Troiani, F., Soldati, M., Notarnicola, C., Savelli, D., Schneiderbauer, S. and Strada, C. (2012) Statistical analysis for assessing shallow-landslide susceptibility in South Tyrol (south-eastern Alps, Italy). Geomorphology **151-152**, 196–206.

Raetzo, H., Lateltin, O., Bollinger, D. and Tripet, J. P. (2002) Hazard assessment in Switzerland – Codes of Practice for mass movements. Bulletin of Engineering Geology and the Environment 2002 61:3 **61**(3), 263–268.

Reichenbach, P., Rossi, M., Malamud, B. D., Mihir, M. and Guzzetti, F. (2018) A review of statistically-based landslide susceptibility models.

Samia, J., Temme, A., Bregt, A., Wallinga, J., Guzzetti, F. and Ardizzone, F. (2020) Dynamic path-dependent landslide susceptibility modelling. Natural Hazards and Earth System Sciences **20**(1), 271–285.

Schlögel, R., Kofler, C., Gariano, S. L., Van Campenhout, J. and Plummer, S. (2020) Changes in climate patterns and their association to natural hazard distribution in South Tyrol (Eastern Italian Alps). Scientific Reports 2020 10:1 **10**(1), 1–14.

Segoni, S., Rosi, A., Fanti, R., Gallucci, A., Monni, A. and Casagli, N. (2018a) A Regional-Scale Landslide Warning System Based on 20 Years of Operational Experience. Water 2018, Vol. 10, Page 1297 **10**(10), 1297.

Segoni, S., Rossi, G., Rosi, A. and Catani, F. (2014) Landslides triggered by rainfall: A semi-automated procedure to define consistent intensity–duration thresholds. Computers & Geosciences **63**, 123–131.

Segoni, S., Tofani, V., Rosi, A., Catani, F. and Casagli, N. (2018b) Combination of rainfall thresholds and susceptibility maps for dynamic landslide hazard assessment at regional scale. Frontiers in Earth Science p. 85.

Stanley, T. A., Kirschbaum, D. B., Benz, G., Emberson, R. A., Amatya, P. M., Medwedeff, W. and Clark, M. K. (2021) Data-Driven landslide nowcasting at the global scale. Frontiers in Earth Science **9**, 378.

Steger, S., Brenning, A., Bell, R. and Glade, T. (2017) The influence of systematically incomplete shallow landslide inventories on statistical susceptibility models and suggestions for improvements. Landslides **14**(5), 1767–1781.

Steger, S., Brenning, A., Bell, R., Petschko, H. and Glade, T. (2016) Exploring discrepancies between quantitative validation results and the geomorphic plausibility of statistical landslide susceptibility maps. Geomorphology **262**, 8–23.

Steger, S., Mair, V., Kofler, C., Pittore, M., Zebisch, M. and Schneiderbauer, S. (2021a) Correlation does not imply geomorphic causation in data-driven landslide susceptibility modelling – Benefits of exploring landslide data collection effects. Science of the Total Environment **776**, 145935.

Steger, S., Mair, V., Kofler, C., Pittore, M., Zebisch, M. and Schneiderbauer, S. (2021b) A statistical exploratory analysis of inventoried slide-type movements for south tyrol (italy). Understanding and Reducing Landslide Disaster Risk: Volume 2 From Mapping to Hazard and Risk Zonation 5th pp. 305–311.

Steger, S., Moreno, M., Crespi, A., Zellner, P. J., Gariano, S. L., Brunetti, M. T., Melillo, M., Peruccacci, S., Marra, F., Kohrs, R. et al. (2023) Deciphering seasonal effects of triggering and preparatory precipitation for improved shallow landslide prediction¡? xmltex\break?¿ using generalized additive mixed models. Natural Hazards and Earth System Sciences **23**(4), 1483–1506.

Stingl, V. and Mair, V. (2005) Introduzione alla geologia dell'Alto Adige. Provincia Autonoma di Bolzano-Alto-Adige. ISBN 9788870734089.

Tasser, E., Mader, M. and Tappeiner, U. (2003) Effects of land use in alpine grasslands on the probability of landslides. Basic and Applied Ecology **4**(3), 271–280.

Titti, G., van Westen, C., Borgatti, L., Pasuto, A. and Lombardo, L. (2021) When enough is really enough? on the minimum number of landslides to build reliable susceptibility models. Geosciences **11**(11), 469.

Trigila, A., Iadanza, C., Guerrieri, L. and Hervás, J. (2007) The IFFI project (Italian landslide inventory): Methodology and results. Guidelines for mapping areas at risk of landslides in Europe **23**, 15.

Trigila, A., Iadanza, C. and Spizzichino, D. (2010) Quality assessment of the Italian Landslide Inventory using GIS processing. Landslides **7**(4), 455–470.

Varnes, D. (1978) Slope movement types and processes. In Landslides, Analysis and Control, Transportation Research Board, eds National Research Council (U.S.). Transportation Research Board., R. L. Schuster and R. J. Krizek, chapter 2, p. 234. Washington: National Academy of Sciences. ISBN 9780309028042.

Varnes, D. J. (1984) Landslide hazard zonation: a review of principles and practice. Number 3. Paris: United Nations Economic, Scientific and Cultural Organization UNESCO. ISBN 9789231018954.

Wang, N., Cheng, W., Marconcini, M., Bachofer, F., Liu, C., Xiong, J. and Lombardo, L. (2022) Space-time susceptibility modeling of hydro-morphological processes at the Chinese national scale. Engineering Geology **301**, 106586.

Wang, N., Lombardo, L., Gariano, S. L., Cheng, W., Liu, C., Xiong, J. and Wang, R. (2021) Using satellite rainfall products to assess the triggering conditions for hydro-morphological processes in different geomorphological settings in China. International Journal of Applied Earth Observation and Geoinformation **102**, 102350.

van Westen, C. J., van Asch, T. W. and Soeters, R. (2006) Landslide hazard and risk zonation - Why is it still so difficult? Bulletin of Engineering Geology and the Environment **65**(2), 167–184.

van Westen, C. J., Castellanos, E. and Kuriakose, S. L. (2008) Spatial data for landslide susceptibility, hazard, and vulnerability assessment: An overview. Engineering Geology **102**(3-4), 112–131.

Wood, S. (2006) Generalized Additive Models : An introduction with R. New York: Chapman and Hall/CRC. ISBN 9780429093159.

Zevenbergen, L. W. and Thorne, C. R. (1987) Quantitative analysis of land surface topography. Earth surface processes and landforms **12**(1), 47–56.

Zuur, A. F., Ieno, E. N., Walker, N., Saveliev, A. A. and Smith, G. M. (2009) Mixed effects models and extensions in ecology with R. Statistics for Biology and Health. New York, NY: Springer New York. ISBN 978-0-387-87457-9.